

HI absorption towards nearby compact radio sources

Yogesh Chandola, S.K. Sirothia and D.J. Saikia

National Centre for Radio Astrophysics, TIFR, Pune University Campus, Post Bag 3, Pune 411 007, India

Accepted. Received

ABSTRACT

We present the results of HI absorption measurements towards a sample of nearby Compact Steep-Spectrum (CSS) and Giga-Hertz Peaked Spectrum (GPS) radio sources, the CORALZ sample, using the Giant Metrewave Radio Telescope (GMRT). We observed a sample of 18 sources and find 7 new detections. These sources are of lower luminosity than earlier studies of CSS and GPS objects and we investigate any dependence of HI absorption features on radio luminosity. Within the uncertainties, the detection rates and column densities are similar to the more luminous objects, with the GPS objects exhibiting a higher detection rate than for the CSS objects. The relative velocity of the blueshifted absorption features, which may be due to jet-cloud interactions, are within $\sim -250 \text{ km s}^{-1}$ and do not appear to extend to values over 1000 km s^{-1} seen for the more luminous objects. This could be due to the weaker jets in these objects, but requires confirmation from observations of a larger sample of sources. There appears to be no evidence of any dependence of HI column density on either luminosity or redshift, but these new detections are consistent with the inverse relation between HI column density and projected linear size.

Key words: galaxies: active – galaxies: evolution – galaxies: nuclei – galaxies: jets – radio lines: galaxies

1 INTRODUCTION

Radio observations of various classes of active galactic nuclei (AGN) have revealed a wide scale of structures. For the luminous radio galaxies and quasars these range from the subgalactic-sized Giga-Hertz Peaked Spectrum (GPS) and Compact Steep-Spectrum (CSS) objects (O’Dea 1998) to the giant radio sources which extend over a Mpc in size (e.g. Ishwara-Chandra & Saikia 1999). The GPS sources have convex spectra which peak at $\sim 1 \text{ GHz}$, while the CSS objects may exhibit a flattening or turnover at significantly lower frequencies (e.g. O’Dea 1998). The GPS sources have projected linear sizes $\lesssim 1 \text{ kpc}$, while CSS sources are usually defined to have a projected linear size $\lesssim 15 \text{ kpc}$ ($H_0 = 71 \text{ km s}^{-1} \text{ Mpc}^{-1}$, $\Omega_m = 0.27$, $\Omega_\Lambda = 0.73$; Spergel et al. 2003). In addition, the high-frequency peakers, where the radio spectra peak at frequencies much $> 1 \text{ GHz}$, are likely to exhibit more compact structures (e.g. Orienti et al. 2006). All these sources have steep high-frequency spectra ($\alpha \gtrsim 0.5$, where $S(\nu) \propto \nu^{-\alpha}$) at frequencies beyond their turn-over frequencies. On the basis of their somewhat symmetric radio structures, some of these compact sources have also been referred to as Compact Symmetric Objects or CSOs (e.g. Wilkinson et al. 1994; Taylor et al. 1996; Readhead et al. 1996). It is widely believed from both dynamical and spectral ageing studies that the peaked spectrum objects are

likely to be the youngest with dynamical ages of $\sim 10^2$ to 10^3 yr (e.g. Phillips & Mutel 1982; O’Dea 1998; Polatidis & Conway 2003), which evolve into the CSS objects with ages of $\sim 10^5 \text{ yr}$ (e.g. Murgia et al. 1999), and which in turn evolve into the larger sources which could be over 10^8 yr old (e.g. Jamrozy et al. 2008; Konar et al. 2008).

These young, radio-loud AGN are ideal objects for studying the triggering of radio activity, the early evolution of classical double-lobed radio sources, interactions of the radio jets with the interstellar medium, and AGN feedback which could affect the evolution and formation of galaxies. These sources may also be used as probes of the environments of the central regions and the interstellar medium of the host galaxies via HI 21-cm absorption observations (e.g. van Gorkom et al. 1989; Vermeulen et al. 2003; Pihlström, Conway & Vermeulen 2003; Gupta et al. 2006, and references therein), as well as radio polarisation measurements (e.g. Mantovani et al. 1994; Saikia & Gupta 2003). The absorbing neutral hydrogen could be associated with either the circumnuclear disk and the putative torus or the halo of the host galaxy. Detection of this gas is also important for studying the anisotropy of the radiation field and thereby testing the unified scheme for active galaxies. An understanding of the distribution and kinematics of this gas over a large range of redshifts and/or luminosities can provide valuable infor-

mation on the evolution of its properties with source size (age), radio luminosity and cosmic epoch.

Several recent studies of CSS and GPS objects have demonstrated that H I absorption is seen in ~ 35 per cent of the objects, with the H I column density being anti-correlated with the source size (Vermeulen et al. 2003; Pihlström, Conway & Vermeulen 2003; Gupta et al. 2006). To a first order, the H I gas may be distributed in the form of a disk, but exhibits a variety of line profiles, suggesting significant and sometimes complex motions. van Gorkom et al. (1989) had reported that H I absorption tends to be redshifted relative to the systemic velocity, suggesting infall of gas. However, recent observations show the situation to be more complex. These observations find many sources with substantial blue shifts, suggesting that the atomic gas may also be flowing out, interacting with the jets or rotating around the nucleus (Vermeulen et al. 2003; Gupta et al. 2006). Morganti et al. (2005) report the detection of low optical depth H I gas which may be blue shifted by over $\sim 1000 \text{ km s}^{-1}$, possibly due to jet-cloud interactions.

Gupta et al. (2006) examined and found no evidence of any correlation between H I column density and luminosity or redshift for a sample of CSS and GPS objects with a radio luminosity largely $\geq 10^{25} \text{ W Hz}^{-1}$ at 5 GHz. Their sample was compiled by combining the results of their observations with existing observations in the literature. Since most of these sources were compiled from strong flux-density limited samples, luminosity and redshift were strongly correlated. To study the properties of H I absorbers in lower-luminosity GPS and CSS sources, and also to examine any dependence independently on luminosity and redshift, one needs different samples to fill in the redshift-luminosity plane. With these objectives we observed the Compact Radio sources at Low Redshift (CORALZ) sample, which was compiled by Snellen et al. (2004), with the sources having flux densities larger than 100 mJy at 1400 MHz and angular sizes less than 2 arcsec. Snellen et al. (2004) used the Faint Images of the Radio Sky at Twenty-Centimeters (FIRST) survey (White et al. 1997), the Automated Plate Measuring (APM) machine catalogue (McMahon & Irwin 1992) of the Palomar Observatory Sky Survey (POSS) and their own observations to select radio sources identified with bright galaxies. Further observations led to a sample of 18 sources with redshifts in the range $0.005 < z < 0.16$ which they estimate to be ~ 95 per cent complete (Snellen et al. 2004; de Vries et al. 2009). Almost all the sources are CSS or GPS objects, suitable for studying young radio sources in the nearby Universe. These sources are also significantly weaker than the CSS or GPS objects studied so far (e.g. Gupta et al. 2006 and references therein) making it possible to determine gas properties in sources of low radio luminosity. The median 5 GHz radio luminosity of these sources is ~ 120 times weaker than those studied by Gupta et al. (2006).

In this paper, we present the results of our observations with the Giant Metrewave Radio Telescope (GMRT) of the CORALZ sample. The observations and data analyses are described in Section 2, while the observational results are described in Section 3. The results are discussed in Section 4, and summarized in Section 5.

2 OBSERVATIONS AND DATA ANALYSIS

These observations were made with the GMRT during 2009 December to 2010 February, using a base-band bandwidth of 4 MHz ($\sim 900 \text{ km s}^{-1}$) in the hardware correlator and an integration time of 16s. Each source was observed for ~ 4 to 5 hr including calibration overheads. The 4 MHz bandwidth consisted of 128 spectral channels, giving a spectral resolution of $\sim 7 \text{ km s}^{-1}$. Simultaneously data were also recorded using the software correlator with a wider bandwidth of 16 MHz over 256 channels and integration times of 16s as well as 2s. The data were acquired with a small visibility integration time from the correlator to help in the identification of radio frequency interference (RFI). The frequencies were tuned such that the expected H I absorption line for each source, corresponding to the optical redshifts listed by Snellen et al. (2004) and the NASA Extragalactic Database (NED), were within the observing bands. The flux density and bandpass calibrators were either 3C48, 3C147 or 3C286, and phase calibrators were observed before and after each scan of a source. Observational details are listed in Table 1. The data reduction was mainly done using AIPS++. The data were reduced using an automated pipeline developed by one of us (SS). After applying bandpass corrections on the phase calibrators, gain and phase variations were estimated. The flux density, bandpass, gain and phase calibration from calibrators were applied to the target sources.

While calibrating the data, bad data were flagged at various stages. The data for antennas with high errors (7σ) in antenna-based solutions were examined and flagged over certain time ranges. Some baselines were flagged based on closure errors on the bandpass calibrator. Channel and time-based flagging of data points corrupted by RFI were done using a median filter with a 6σ threshold. Residual errors above 5σ were also flagged after a few rounds of target field calibration (using point source model). Both polarizations (RR and LL) were processed independently for consistency checks. The linear fits (of line free channels) at an interval of 5 minutes were subtracted from the calibrated data. The spectra for the targets were made after averaging the resulting data and correcting for the velocities for the Earth's motion using dopset. Data from both the software and hardware correlator were analysed for consistency checks. The spectra were similar and the ones presented here are from the hardware correlator because it has twice the spectral resolution than those obtained from the software correlator data. The typical channel r.m.s. for the spectra presented here are $\sim 1.3 \text{ mJy}$.

3 OBSERVATIONAL RESULTS

3.1 H I observations

Some of the basic properties of the sample of sources and the observational results are summarized in Table 2, which is largely self explanatory. The classification of GPS and CSS sources are based on the spectra presented by Snellen et al. (2004) and any additional information from Labiano et al. (2007). Sources with a reasonably well-defined spectral peak at frequencies $\gtrsim 500 \text{ MHz}$ have been classified as GPS, while the others have been termed as CSS objects. J102618+454618 has been classified as CFS (Compact Flat

Table 1. Observational details of the GMRT search for HI absorption in the CORALZ sample.

Source Name	Date	COB ¹ Freq MHz	Total Observation time hr	Flux density and Bandpass Calibrator	Phase Calibrator
J073328+560541	2009 Dec 31	1286.5	5	3C147	J0713+438
J073934+495438	2010 Jan 05	1347.5	5	3C286	J0713+438
J083139+460800	2010 Jan 05	1260.0	5	3C286	J0713+438
J083637+440109	2010 Jan 04	1346.0	4	3C286	J0713+438
J090615+463618	2010 Feb 03	1309.0	5	3C286	J0713+438
J102618+454229	2010 Jan 02	1232.0	5	3C147	J1219+484
J103719+433515	2009 Dec 29	1388.5	5	3C286	J1219+484
J115000+552821	2010 Jan 03	1247.3	5	3C286	3C286
J120902+411559	2010 Jan 01	1297.0	5	3C147	J1227+365
J131739+411545	2009 Dec 29	1332.5	5	3C286	J1227+365
J140051+521606	2010 Jan 27	1270.5	5	3C286	3C286
J140942+360416	2010 Jan 03	1237.0	5	3C286	3C286
J143521+505122	2010 Jan 02	1292.5	5	3C286	3C286
J150805+342323	2010 Jan 01	1359.0	5	3C286	3C286
J160246+524358	2010 Jan 04	1284.5	4	3C286	J1634+627
J161148+404020	2010 Feb 09	1233.0	5	3C286	J1613+342
J170330+454047	2009 Dec 11	1340.0	5	3C286	J1613+342
J171854+544148	2010 Feb 02	1238.5	5	3C48	J1634+627

¹ COB Freq: Centre of Band Frequency before any correction for velocity using dopset

Spectrum) because it appears to have a high-frequency spectral index of ~ 0.41 (Snellen et al. 2004; de Vries et al. 2009). From observations of the sources in the CORALZ sample with the GMRT, we report the detection of HI absorption in 7 sources, of which 3 are GPS sources and 4 are CSS objects (Table 2). The detected absorption lines were fitted with multiple Gaussian components to determine the peak optical depth τ_p and FWHM (Δv ; km s⁻¹) of the spectral components. HI column densities were determined using the relation

$$\begin{aligned}
 N(\text{HI}) &= 1.835 \times 10^{18} \frac{T_s \int \tau(v) dv}{f_c} \text{ cm}^{-2} \\
 &= 1.93 \times 10^{18} \frac{T_s \tau_p \Delta v}{f_c} \text{ cm}^{-2}
 \end{aligned} \quad (1)$$

where T_s and f_c are the spin temperature (in K) and the fraction of the background source covered by an absorbing cloud. We have assumed $T_s=100$ K and $f_c=1.0$. The column densities range from $\sim 1.78 \times 10^{20}$ to $\sim 10^{22}$ cm⁻², with a median value of $\sim 7 \times 10^{20}$ cm⁻². These values are similar to those of the more luminous GPS and CSS sources where the median value is $\sim 5 \times 10^{20}$ cm⁻² (Gupta et al. 2006).

For the non-detections, we have determined the upper limits on HI column densities using $3 \times \text{r.m.s.}$ of the optical depths as τ_p and $\Delta v=100$ km s⁻¹. These upper limits range from ~ 0.9 to $\sim 4.2 \times 10^{20}$ cm⁻². The spectra for the non-detections are shown in Fig. 1, while the spectra for the detections are presented in Fig. 2 along with the Gaussian fits to the optical depths. All the spectra have been plotted relative to the systemic velocity inferred from the redshifts listed in Table 2, which are from NED, but taken mainly from the Sloan Digital Sky Survey (SDSS; Adelman-McCarthy et al. 2008, and references therein), except for J083139+460800 and J103719+433515 which have been plotted relative to the redshifts listed by Snellen et al. (2004). For all the non-detections, the absence of HI absorption has also been con-

firmed from the wider bandwidth software correlator data, except for J103719+433515, where there was an error in the settings. We describe below each source briefly including J083139+460800 and J103719+433515, which is then followed by the discussion Section.

3.2 Notes on individual sources

J073328+560541: Very Long Baseline Interferometric (VLBI) images at ~ 1.6 and 5 GHz show the source to have an extent of ~ 80 mas (Bondi et al. 2001; de Vries et al. 2009), while Very Large Array A-array observations at 8.4 GHz show an unresolved source with an angular extent < 0.2 arcsec (Patnaik et al. 1992). The location of the core is unclear and the source is unpolarized (Bondi et al. 2004). Goncalves & Serote Roos (2004) suggest the presence of Low Ionization Nuclear Emission-line Region (LINER), while Dennett-Thorpe & Marchã (2000) suggest that the source might be variable at 1.4 GHz. The radio spectrum peaks at ~ 460 MHz (Snellen et al. 2004). We do not find evidence of HI absorption.

J073934+495438: VLBI images of the source at ~ 5 GHz show it to be unresolved (de Vries et al. 2009). The radio spectrum peaks at ~ 950 MHz (Snellen et al. 2004). We do not find evidence of HI absorption.

J083139+460800: VLBI observations show the source to be double lobed with an overall separation of 4.4 mas in the image of epoch 2000, while a weak component visible towards the north in the image of epoch 2004 gives an overall size of ~ 9 mas (de Vries et al. 2009). The redshift of the host galaxy from SDSS is 0.1311, while Snellen et al. (2004) list it as 0.127. It is a GPS source with a turnover at ~ 2200 MHz (Snellen et al. 2004). We do not find evidence of HI absorption. In the spectrum shown in Fig. 1, zero velocity corresponds to optical redshift of 0.127 listed by Snellen et al. (2004) and de Vries et al. (2009). While

Table 2. Characteristics of sources in the CORALZ sample. The redshifts, z , are from NED with the original references being listed in Column 4, while the flux densities are from the FIRST survey. The luminosities from Snellen et al. (2004) have been re-estimated in the cosmology used here. The largest angular sizes (θ) are from de Vries et al. (2009) except for J073328+560541 (Bondi et al. 2001) and J170330+454047 (Gu & Chen 2010). LS denotes the corresponding linear sizes.

Source Name (1)	Opt Id. (2)	z (3)	Refs. (4)	$S_{1.4GHz}$ mJy (5)	L_{5GHz} $10^{25} (W Hz^{-1})$ (6)	θ (mas) (7)	LS (pc) (8)	Spectral Class (9)	N(HI) $10^{20} cm^{-2}$ (10)
J073328+560541	G	0.1040	1	348	0.467	80	151	GPS	<1.076
J073934+495438	G	0.0540	1,2	107	0.042	<2	<2.1	GPS	<2.097
J083139+460800	G	0.1311	3	131	0.408	9	20.7	GPS	<1.256
J083637+440109	G	0.0554	3	139	0.045	1600	1699	CSS	<1.945
J090615+463618	G	0.0848	1,3	314	0.302	31	48.9	GPS	7.482
J102618+454618	G	0.1517	3	105	0.347	17	44.7	CFS	<3.617
J103719+433515	G	0.0247	3,4	129	0.009	19	8.7	CSS	<1.932
J115000+552821	G	0.1385	3	143	0.363	41	93.9	CSS	6.31
J120902+411559	G	0.0950	2	147	0.178	20	34.8	CSS	<1.854
J131739+411545	G	0.0662	1,3	249	0.229	4	5	GPS	3.785
J140051+521606	G	0.1180	3	174	0.224	<150	<316	CSS	<1.139
J140942+360416	G	0.1484	3	143	0.276	27	69.2	CSS	7.667
J143521+505122	G	0.0997	3	141	0.155	<150	<271	CSS	<2.339
J150805+342323	G	0.0456	5	130	0.022	170	148	CSS	125.183
J160246+524358	G	0.1057	3	576	0.549	180	345	CSS	1.781
J161148+404020	G	0.1520	2	553	1.048	1300	3400	CSS	<0.929
J170330+454047	G	0.0604	6	119	0.034	<7.3	<8.4	CSS	<4.165
J171854+544148	G	0.1470	1,7	329	0.617	68	172.9	GPS	9.541

References for redshifts: 1 Labiano et al. (2007); 2 Snellen et al. (2004); 3 SDSS (Adelman-McCarthy et al. 2008 and references therein); 4 Falco et al. (1999); 5 Mazzarella et al. (1993); 6 de Grijs et al. (1992); 7 Kim & Sanders (1998)

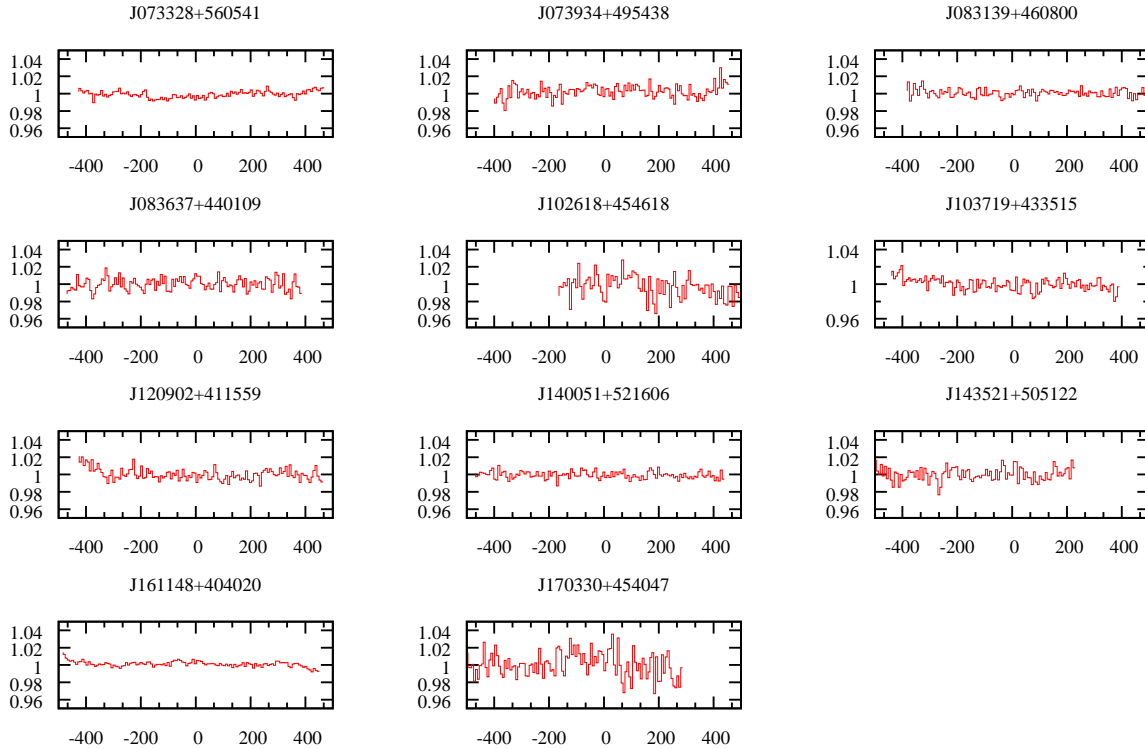


Figure 1. GMRT spectra for the non-detections. The y-axis shows the normalised intensity while the x-axis shows the velocity in $km s^{-1}$.

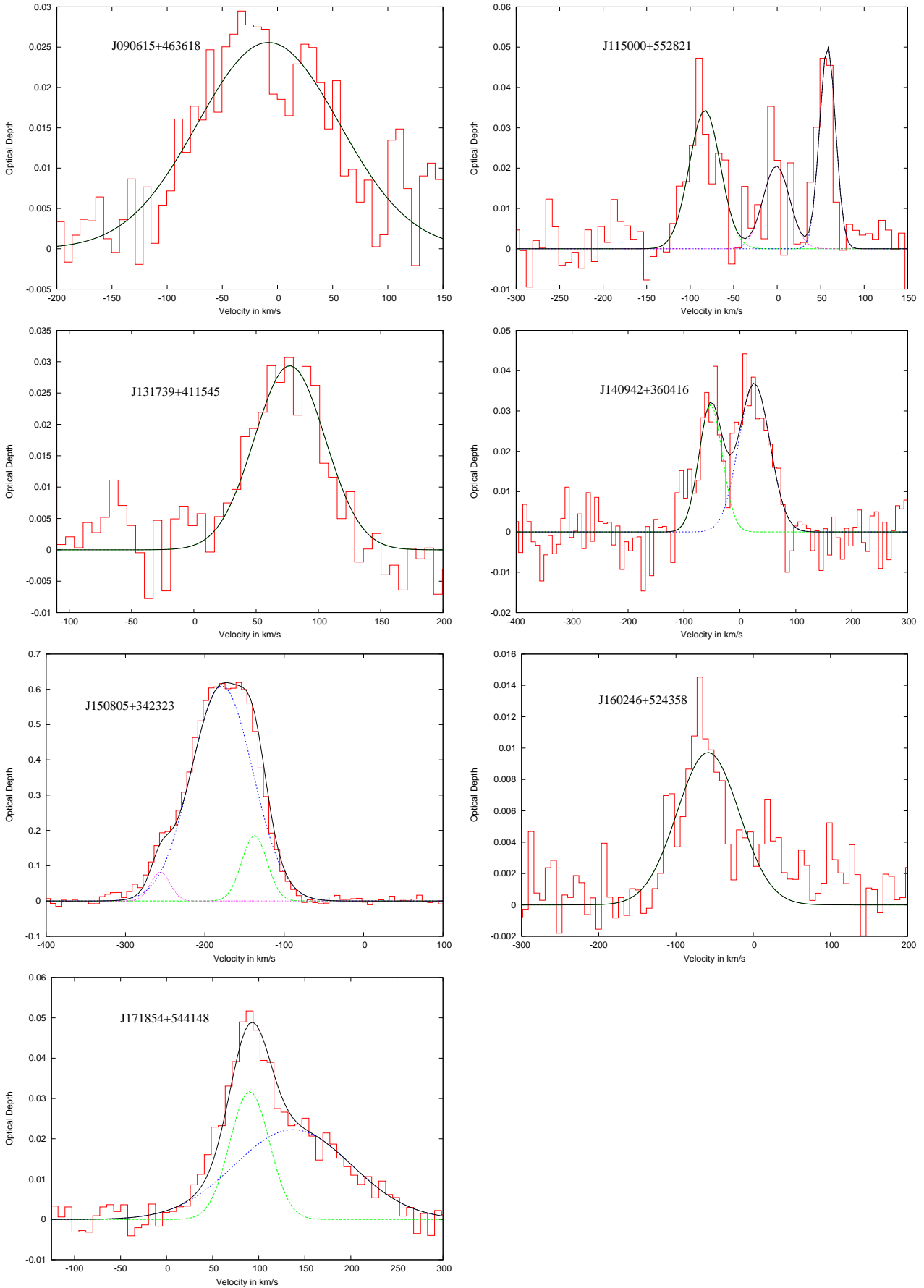


Figure 2. The optical depth of the H I absorbers vs velocity in km s^{-1} relative to the systemic velocity.

the redshift of 0.1311 is not within the range covered by the hardware correlator, it is within the range covered by the software correlator and no HI absorption is seen.

J083637+440109: The MERLIN image at 1.6 GHz (de Vries et al. 2009) shows most of the emission to form a C-shaped structure with an angular size of ~ 1600 mas. We do not find evidence of HI absorption.

J090615+463618: The radio structure revealed by the VLBI maps (de Vries et al. 2009; Helmboldt et al. 2007) has been suggested to be due to emission on opposite sides of the core by Bondi et al. (2004). The source exhibits no significant polarization at both radio ($<0.99\%$) and optical ($<1.2\%$) wavelengths (Marchã et al. 1996; Dennett-Thorpe & Marchã 2000). Caccianiga et al. (2002) classify it as a Narrow Emission Line Galaxy, while Goncalves & Serote Roos (2004) suggest it to be a LINER. We detect HI absorption in this source with one main component blueshifted by ~ 8 km s $^{-1}$ (Fig. 2) for which the Gaussian fit parameters are given in Table. 3.

J102618+454618: The VLBI map at 5 GHz (de Vries et al. 2009), has multiple components with an overall separation of 17 mas, with the central feature being the most prominent one. From the VLBI maps at 1665 and 4993 MHz (de Vries et al. 2009), the central feature has a flat spectra. We do not find evidence of HI absorption.

J103719+433515: This source too has an elongated structure with multiple components and an overall size of 19 mas. The brightest component in the central region of the source appears to have a flat spectrum (de Vries et al. 2009). There is no evidence of HI absorption. The zero velocity in the spectrum corresponds to the optical redshift of 0.023 as given by Snellen et al. (2004), while the one given by NED is 0.0247 (Falco et al. 1999), which was not covered by the hardware correlator. There was also an error in the settings of the software correlator. The source needs to be re-observed to ensure that there is also no absorption at a redshift of 0.0247. For the present, we have classified it as a non-detection.

J115000+552821: The VLBI map at 1.6 GHz shows a dominant compact component with weak emission towards the east separated from it by ~ 41 mas (de Vries et al. 2009). We detect HI absorption, with three components (Fig. 2), one of which is redshifted and one blueshifted relative to the systemic velocity. The third one, which is weaker and would be useful to confirm, is consistent with the systemic velocity. The Gaussian fitting parameters are given in Table. 3.

J120902+411559: The source exhibits multiple components with a prominent central feature and is elongated along the east-west direction with angular size ~ 20 mas (de Vries et al. 2009). The radio spectrum of this source peaks at 370 MHz (Snellen et al. 2004). There is no evidence of HI absorption.

J131739+411545: VLBI maps show a complex structure with size of ~ 4 mas (Helmboldt et al. 2007; de Vries et al. 2009). The radio spectrum of this source peaks at 2.3 GHz (Snellen et al. 2004). We detect HI absorption, where the line profile is redshifted with respect to the optical redshift by 77 km s $^{-1}$ indicating infall of gas towards the central source (Fig. 2). The Gaussian fit parameters are listed in Table 3.

J140051+521606: The MERLIN map at 1.4 GHz shows a resolved component with a deconvolved angular size of

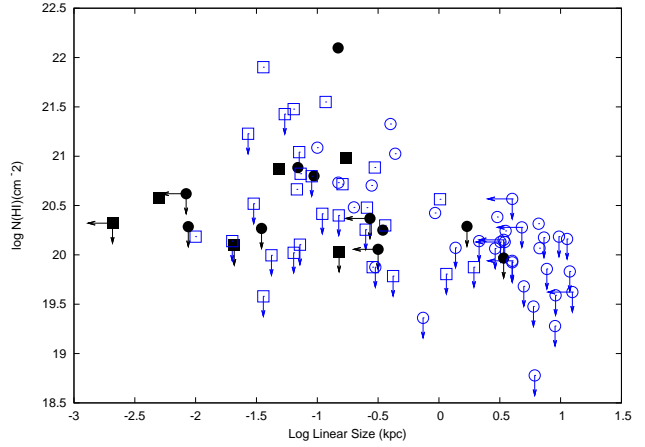


Figure 3. HI column density versus projected linear size for the CORALZ sample as well as the higher luminosity CSS and GPS objects. The black filled symbols denote the CORALZ sources, while blue open symbols denote the sources from the Gupta et al. (2006) compilation. CSS and GPS sources are represented by circles and squares respectively.

182.3 \times 95.9 mas along a PA of 102 $^\circ$ (Table B2 of de Vries et al. 2009). There is no evidence of HI absorption.

J140942+360416: The VLBI images at ~ 1.7 GHz suggest that it could be a very asymmetric double. The higher resolution image in de Vries et al. (2009) shows the component towards the north to have a weaker flux density by a factor of ~ 10 . The radio spectrum of this source peaks at 330 MHz (Snellen et al. 2004). We detect HI absorption towards this source. The HI line profile shows two components, one blueshifted while the second one is redshifted relative to the systemic velocity, consistent with rotation of the absorbing gas (Fig. 2; Table 3).

J143521+505122: The MERLIN image at 1.4 GHz shows extended emission which has been deconvolved into two well-resolved components (de Vries et al. 2009). There is no detection of HI absorption.

J150805+342323: The VLBI map at 1.6 GHz shows two components. (de Vries et al. 2009). CO emission has been detected from this source (Mazzarella et al. 1993; Evans et al. 2005). There is evidence of strong HI absorption (Fig. 2; Table 3). The Gaussian fit to the optical depth and velocity shows blueshifted gas with three main components which could be due to outflowing gas.

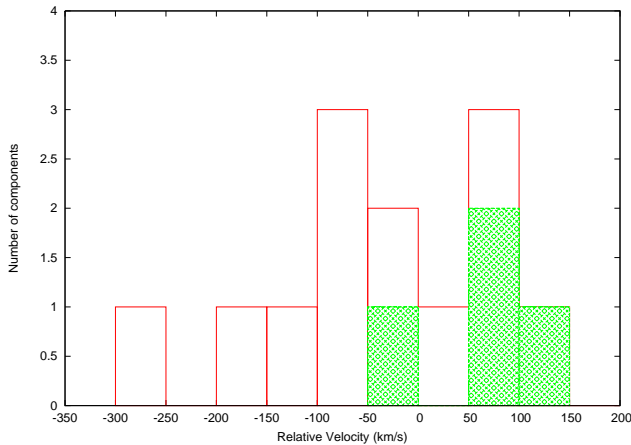
J160246+524358: The VLBI map at 5 GHz (de Vries et al. 2009) shows a compact flat-spectrum core with jet-like emission on opposite sides. The optical source has been classified as a Seyfert 1 AGN by Véron & Véron (2006). There is evidence of blueshifted HI absorbing gas (Fig 2; Table 3).

J161148+404020: The complex structure of this source is seen in a MERLIN map at 1.6 GHz with an overall angular size of 1300 milliarcsec (de Vries et al. 2009). There is no detection of HI absorption.

J170330+454047: This is a compact unresolved radio source as observed in the Japanese VLBI Network map at 8.4 GHz (Doi et al. 2007), while VLBA map at 5 GHz shows two components resolved into core-jet (Gu & Chen 2010). This source was classified originally as Seyfert 2 (de Grijs et al. 1992) but later on reclassified as a Narrow Line Seyfert

Table 3. Multiple Gaussian fit parameters to the HI absorption spectra for the detections.

Object	Component Number	Vel km s ⁻¹	FWHM km s ⁻¹	τ_p	N(HI) 10 ²⁰ cm ⁻²
J090615+463618	1	-8.2(4.2)	151.5(10.1)	0.0256(0.0015)	7.48(0.93)
J115000+552821	1	-83.1(2.6)	42.1(6.1)	0.0343(0.0043)	2.79(0.76)
	2	-0.9(4.0)	36.0(9.6)	0.0206(0.0047)	1.43(0.71)
	3	57.9(1.3)	21.5(3.0)	0.0504(0.0060)	2.09(0.54)
J131739+411545	1	77.0(2.4)	66.8(5.8)	0.0294(0.0022)	3.79(0.61)
J140942+360416	1	-52.2(3.4)	49.2(7.9)	0.0316(0.0033)	3.00(0.80)
	2	25.7(3.3)	65.6(8.4)	0.0369(0.0029)	4.67(0.97)
J150805+342323	1	-256.1(1.4)	28.8(3.6)	0.0822(0.0083)	4.56(1.04)
	2	-178.4(1.1)	91.1(1.7)	0.6100(0.0084)	107.20(3.46)
	3	-137.5(0.9)	37.4(3.1)	0.1862(0.0178)	13.42(2.39)
J160246+524358	1	-58.4(4.2)	94.9(9.8)	0.0097(0.0009)	1.78(0.34)
J171854+544148	1	90.1(1.4)	50.6(4.2)	0.0317(0.0024)	3.10(0.49)
	2	137.2(5.7)	149.9(10.9)	0.0223(0.0019)	6.44(1.01)


Figure 4. The distribution of the velocity of the different HI absorbing components relative to the systemic velocities of the host galaxies. The GPS sources are shown shaded.

1 (Moran et al. 1996; Wisotzki & Bade 1997). There is no evidence of HI absorption.

J171854+544148: This source shows two prominent components with a separation of ~ 68 mas at ~ 1.6 GHz, reminiscent of a CSO, but shows two weaker components in a higher-resolution image at ~ 5 GHz (de Vries et al. 2009). This source has been classified as a Seyfert type 2 (Veilleux et al. 1999). It was earlier classified by Leech et al. (1994) as an interacting system, but the second object appears to be a foreground star (Bruston, Ward & Davies 2001; Davies, Burston & Ward 2002). The object is also associated with an ultraluminous infrared galaxy (ULIRG) F17179+5444 (Leech et al. 2004). The radio spectrum of the source peaks at ~ 480 MHz. We detect HI absorption towards this source (Fig. 2; Table 3), with two main components, both of which are redshifted relative to the systemic velocity.

4 DISCUSSION

The radio luminosity of the sources in the core CORALZ sample which have a flux density at 1400 MHz > 100 mJy, redshift in the range 0.005 to 0.16 and angular size < 2 arcsec (Snellen et al. 2004; de Vries et al. 2009) are almost always less than $\sim 10^{25}$ W Hz⁻¹ at 5 GHz. Since the radio luminosities of 95 per cent of the sources in the sample compiled by Gupta et al. (2006) are greater than $\sim 10^{25}$ W Hz⁻¹ at 5 GHz, we have compared our results with those of Gupta et al. (2006) to examine any broad dependence on radio luminosity. In this section, we leave out J102618+454618 which has a flat high-frequency spectrum (Snellen et al. 2004). In the remaining sample of 17 compact low redshift sources, we were able to detect 7 new sources in HI absorption. Of these seven, three are GPS and four are CSS sources, the fraction of detection for the GPS sources being ~ 50 per cent (3/6) compared with ~ 36 per cent (4/11) for CSS objects. Although the numbers are small and statistical uncertainties are large, these are consistent with the detection rates for the more luminous sources, and the tendency for GPS objects to have a higher detection rate compared with CSS objects (e.g. Vermeulen et al. 2003; Pihlström et al. 2003; Gupta et al. 2006). As mentioned earlier in Section 3.1, the column densities are similar to those for the more luminous CSS and GPS objects.

4.1 HI column density vs linear size

Earlier studies have shown an inverse correlation between the HI column density and the projected linear size. This was first noticed by Pihlström et al. (2003) and was later shown to be also true for a significantly larger sample of sources by Gupta et al. (2006). In Fig. 3 we have plotted the results of our observations for these 17 sources in the HI column density vs linear size diagram, along with the list of higher-luminosity sources compiled by Gupta et al. (2006). These

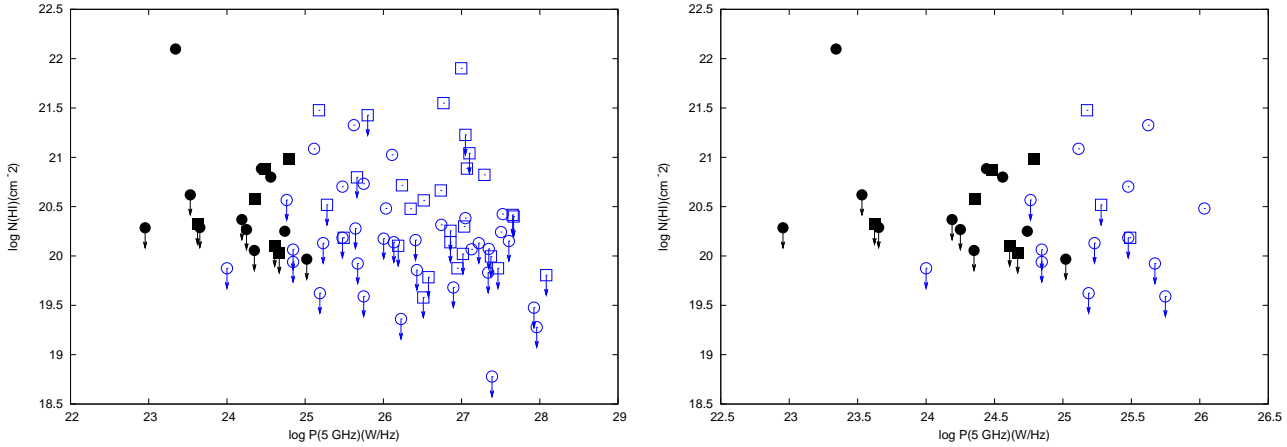


Figure 5. Left panel: H I column density versus source luminosity at 5 GHz for the CORALZ sample (black filled ones) and from the Gupta et al. (2006) compilation (blue open ones). The CSS and GPS objects are shown by circles and squares respectively. Right panel: Same as left but for sources with a redshift < 0.2 .

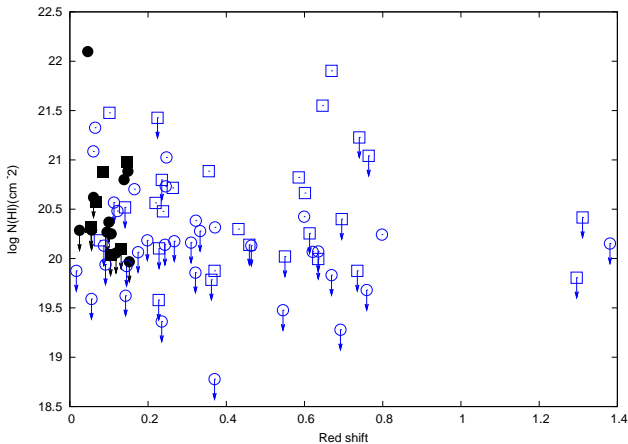


Figure 6. H I Column density versus redshift for the CORALZ sources (black filled symbols) and the CSS and GPS objects from the compilation by Gupta et al. (2006) shown with open blue symbols. The CSS and GPS objects are shown by circles and squares respectively.

low-luminosity radio sources from the CORALZ sample are consistent with a similar relationship, suggesting that the most compact sources are seen through regions of higher column density.

4.2 Relative velocity of H I absorption features

The distribution of the relative velocity for the H I absorbing components listed in Table 3 is shown in Fig. 4. These range from ~ -250 to 140 km s^{-1} , with a median value of $\sim -50 \text{ km s}^{-1}$. Although the number of absorption features is small, and there are uncertainties in the systemic velocities (e.g. Morganti et al. 2001) there appears to be a marginal trend for a higher number of blueshifted features.

Although blueshifted H I absorption features could also arise from either halo or circumnuclear gas affected by winds and/or radiation pressure from the nuclear region, jet-cloud

interactions are likely to significantly affect the gas properties in compact steep-spectrum radio sources. The tendency for CSS and GPS objects to be more asymmetric in location, brightness and polarization of the lobes compared with the larger objects suggest strong interaction of the jets with the circumnuclear region (e.g. Saikia et al. 1995, 2001; Arshakian & Longair 2000; Saikia & Gupta 2003). Rotation measure (RM) studies also indicate high values in many compact sources (e.g. Mantovani et al. 1994, 2010; O’Dea et al. 1998), often with large asymmetries in the RM values for the oppositely-directed lobes due to interaction with asymmetrically located clouds of gas (e.g. Junor et al. 1999). Evidence of interaction is also seen in optical emission and absorption line studies (e.g. Gelderman & Whittle 1994; Chatzichristou et al. 1999; Labiano et al. 2005; Gupta et al. 2005).

Excess of blueshifted absorption features has been reported earlier. For example, for a sample of quasars Baker et al. (2002) found a small excess of blueshifted C IV absorption features in CSS objects compared with the larger sources which they attribute to absorbing material being away from the jet axis, whereas van Ojik et al. (1997) found an excess of blueshifted Ly α absorption features in their sample of small-sized high-redshift radio galaxies which they attribute to absorbing clouds uniformly covering the whole source signifying a halo origin. The sample of CSS and GPS objects compiled by Gupta et al. (2006) also shows a tendency for the H I absorption features to be blueshifted with velocities extending to over 1000 km s^{-1} . Although the number of low-luminosity sources needs to be increased, the present observations suggest that the blueshifted velocities in these low-luminosity sources could be smaller possibly due to the weaker radio jets in these objects.

4.3 H I column density vs luminosity and redshift

It is generally believed that AGN activity is triggered by the accretion of matter onto a supermassive blackhole at the centre of the galaxy. Mergers and interactions of galax-

ies could facilitate the supply and inflow of gas into the central regions of these active galaxies leading to both circumnuclear starbursts and fuelling the supermassive black-holes (e.g. Sanders et al. 1988; Hopkins et al. 2005). It may therefore be relevant to investigate whether the HI column density may depend on either radio luminosity or redshift. Gupta et al. (2006) did not find any evidence of such relationships in their sample of luminous CSS and GPS objects. However, since most of the sources in their sample were selected from strong-source surveys, luminosity and redshift are strongly correlated. Constraining the sources from the Gupta et al. (2006) sample to those with redshifts <0.2 , we have examined any dependence of column density on luminosity over a similar redshift range but find no evidence of any significant relationship (Fig. 5). The CORALZ sources are of lower luminosity than the Gupta et al. (2006) sample making it difficult to examine variation with redshift for similar luminosity objects. We have plotted the HI column density vs redshift for the CORALZ sources along with all the sources from the Gupta et al. (2006) sample (Fig. 6) and find no evidence of any correlation.

5 SUMMARY

The results of HI absorption measurements towards a sample of nearby CSS and GPS radio sources, the CORALZ sample, using the GMRT are summarized briefly here. These sources are of lower luminosity than earlier studies of CSS and GPS objects.

(i) We observed a sample of 18 sources and find 7 new detections. Within the uncertainties caused by the small sample size, the detection rates are similar to the more luminous objects, with the GPS objects again exhibiting a higher detection rate (3/6) than for CSS objects (4/11).

(ii) The relative velocity of the blueshifted absorption features, which may be due to jet-cloud interactions, extend to only ~ 250 km s $^{-1}$ for these CORALZ sources compared with values of over ~ 1000 km s $^{-1}$ for the more luminous CSS and GPS objects. This could be due to the weaker jets in these low-luminosity objects, although this needs confirmation from a larger sample of objects.

(iii) There appears to be no evidence of any dependence of HI column density on either luminosity or redshift. Examining sources over a similar redshift range (<0.2) also shows no evidence of any correlation with luminosity.

(iv) The weaker CSS and GPS objects are also consistent with the known inverse relation of HI column density with projected linear size.

ACKNOWLEDGMENTS

We thank the reviewer for his/her detailed and valuable comments which have helped improved the manuscript significantly. We thank the staff of GMRT for their assistance during our observations. The GMRT is a national facility operated by the National Centre for Radio Astrophysics of the Tata Institute of Fundamental Research. We thank numerous contributors to the GNU/Linux group. This research has made use of the NASA/IPAC Extragalactic Database

(NED) which is operated by the Jet Propulsion Laboratory, California Institute of Technology, under contract with the National Aeronautics and Space Administration. We have made use of the cosmological calculator by Edward L. Wright (Wright 2006). This research has made use of NASA's Astrophysics Data System.

REFERENCES

- Arshakian T.G., Longair M.S., 2000, MNRAS, 311, 846
- Adelman-McCarthy et al. 2008, ApJS, 175, 297
- Baker J.C., Hunstead R.W., Athreya R.M., Barthel P.D., de Silva E., Lehnert M.D., Saunders R.D.E., 2002, ApJ, 568, 592
- Bondi M., Marchã M.J.M., Dallacasa D., Stanghellini C., 2001, MNRAS, 325, 1109
- Bondi M., Marchã M.J.M., Polatidis A., Dallacasa D., Stanghellini C., Antón S., 2004, MNRAS, 352, 112
- Bruston A.J., Ward M.J., Davies R.I., 2001, MNRAS, 326, 403
- Caccianiga A., Marchã M.J., Antón S., Mack K.-H., Neeser M.J., 2002, MNRAS, 329, 877
- Chatzichristou E.T., Vanderriest C., Jaffe W., 1999, A&A, 343, 407
- Davies R.I., Burston A.J., Ward M.J., 2002, MNRAS, 329, 367
- de Grijp M.H.K., Keel W.C., Miley G.K., Goudfrooij P., Lub J., 1992, A&AS, 96, 389
- Dennett-Thorpe J., Marchã M.J., 2000, A&A, 361, 480
- Doi A., et al., 2007, PASJ, 59, 703
- de Vries N., Snellen I.A.G., Schilizzi R.T., Mack K.H., Kaiser C.R., 2009, A&A, 498, 641
- Evans A.S., Mazzarella J.M., Surace J.A., Frayer D.T., Iwasawa K., Sanders D.B., 2005, ApJ, 159, 197
- Falco E.E., et al., 1999, PASP, 111, 438
- Gelderman R., Whittle M., 1994, ApJS, 91, 491
- Goncalves A.C., Serote Roos M., 2004, A&A, 413, 97
- Gu M., Chen Y., 2010, AJ, 139, 2612
- Gupta N., Srianand R., Saikia D.J., 2005, MNRAS, 361, 451
- Gupta N., Salter C.J., Saikia D.J., Ghosh T., Jeyakumar S., 2006, MNRAS, 373, 972
- Helmboldt J.F., et al., 2007, ApJ, 658, 203
- Hopkins P.F., Hernquist L., Cox T.J., Di M.T., Martini P., Robertson B., Springel V., 2005, ApJ, 630, 705
- Ishwara-Chandra C.H., Saikia D.J., 1999, MNRAS, 309, 100
- Jamrozny M., Konar C., Machalski J., Saikia D.J., 2008, MNRAS, 385, 1286
- Junor W., Salter C.J., Saikia D.J., Mantovani F., Peck A.B., 1999, MNRAS, 308, 955
- Kim D.-C., Sanders D.B., 1998, ApJS, 119, 41
- Konar C., Jamrozny M., Saikia D.J., Machalski J., 2008, MNRAS, 383, 525
- Labiano A., et al., 2005, A&A, 436, 493
- Labiano A., Barthel P.D., O'Dea C.P., de Vries W.H., Pérez I., Baum, S.A., 2007, A&A, 463, 97
- Leech K.J., Rowan-Robinson M., Lawrence A., Hughes J.D., 1994, MNRAS, 267, 253
- Mantovani F., Junor W., Fanti R., Padrielli L., Saikia D.J., 1994, A&A, 922, 59
- Mantovani F., Rossetti A., Junor W., Saikia D.J., Salter C.J., 2010, A&A, 518, A33
- Marchã M.J.M., Browne I.W.A., Impey C.D., Smith P.S., 1996, MNRAS, 281, 425
- Mazzarella J.M., Graham J.R., Sanders D.B., Djorgovski S., 1993, ApJ, 409, 170
- McMahon R.G., Irwin M.J., 1992, ASSL, 174, 417
- Moran Edward C., Halpern Jules P., Helfand David J., 1996, ApJS, 106, 341
- Morganti R., Oosterloo T.A., et al., 2001, MNRAS, 323, 331

- Morganti R., Tadhunter C.N., Oosterloo T.A., 2005, *A&A*, 444, 99
- Murgia M., Fanti C., Fanti R., Gregorini L., Klein U., Mack K.-H., Vigotti M., 1999, *A&A*, 345, 769
- O'Dea C.P., 1998, *PASP*, 110, 493
- O'Dea C.P., Baum S.A., Stanghellini C., 1991, *ApJ*, 380, 660
- Orienti M., Dallacasa D., Tinti S., Stanghellini C., 2006, *A&A*, 450, 959
- Patnaik A.R., Browne I.W.A., Wilkinson P.N., Wrobel J.M., 1992, *MNRAS*, 254, 655
- Phillips R.B., Mutel R.L., 1982, *A&A*, 106, 21
- Pihlström Y.M., Conway J.E., Vermeulen R.C., 2003, *A&A*, 404, 871
- Polatidis A.G., Conway J.E., 2003, *PASA*, 20, 69
- Rees M.J., 1984, *ARA&A*, 22, 471
- Readhead A.C.S., Taylor G.B., Pearson T.J., Wilkinson P.N., 1996, *ApJ*, 460, 634
- Saikia D.J., Gupta N., 2003, *A&A*, 405, 499
- Saikia D.J., Jeyakumar S., Wiita P.J., Sanghera H.S., Spencer R.E., 1995, *MNRAS*, 276, 1215
- Saikia D.J., Jeyakumar S., Salter C.J., Thomasson P., Spencer R.E., Mantovani F., 2001, *MNRAS*, 321, 37
- Sanders D.B., Soifer B.T., Elias J.H., Neugebauer G., Matthews K., 1988, *ApJ*, 328, 35
- Snellen I.A.G., Mack K.-H., Schilizzi R.T., Tschager W., 2004, *MNRAS*, 348, 227
- Spergel D.N., et al., 2003, *ApJS*, 148, 175
- Taylor G.B., Readhead A.C.S., Pearson T.J., 1996, *ApJ*, 463, 95
- van Gorkom J.H., Knapp G.R., Ekers R.D., Ekers D.D., Laing R.A., Polk K.S., 1989, *AJ*, 97, 708
- van Ojik R., Röttgering H.J.A., Miley G.K., Hunstead R.W., 1997, *A&A*, 317, 358
- Veilleux S., Kim D.-C., Sanders D.B., 1999, *ApJ*, 522, 113
- Vermeulen R.C., et al., 2003, *A&A*, 404, 861
- Véron-Cetty M.-P., Véron P., 2006, *A&A*, 455, 773
- White R.L., Becker R.H., Helfand D.J., Gregg M.D., 1997, *ApJ*, 475, 479
- Wilkinson P.N., Polatidis A.G., Readhead A.C.S., Xu W., Pearson T.J., 1994, *ApJ*, 432, 87
- Wisotzki L., Bade N., 1997, *A&A*, 320, 395
- Wright E.L., 2006, *PASP*, 118, 1711